Multiply charged ion acceleration studies using the Vulcan Petawatt laser

P. McKenna, D. C. Carroll, L. Robson*, K. W. D. Ledingham and T. McCanny
SUPA, Department of Physics, University of Strathclyde, Glasgow, G4 0NG, UK

F. Lindau, O. Lundh and C.-G. Wahlström
Department of Physics, Lund Institute of Technology, P.O. Box 118, 221 00 Lund, Sweden

A. P. L. Robinson, R. J. Clarke and D. Neely
Central Laser Facility, STFC, Rutherford Appleton Laboratory, Chilton, Didcot, Oxon, OX11 0QX, UK

P. T. Simpson and M. Zepf
Department of Physics and Astronomy, Queens University Belfast, Belfast, BT7 1NN, UK

* Also at AWE plc Aldermaston, Reading RG7 4PR, UK

Main contact email address **p.mckenna@phys.strath.ac.uk**

Introduction

Multiply-charged ion acceleration has been investigated using long (~ns) and, recently, short (ps and sub-ps) laser pulses[1,2]. Using 1 ps duration pulses focused to subrelativistic intensities of ~5×10^{16} W/cm^2, Ta and Au ions with charge states up to 38+ and 33+, respectively, and energy of the order of 1 MeV, have been demonstrated[3]. Skin-Layer Ponderomotive Acceleration (S-LPA) is the main acceleration mechanism of the backward-directed ions investigated in these studies. Multiply charged fast ions generated by ultraintense laser pulses have also been investigated, for both forward-[4-7] and backward-directed beams[8,9]. The main acceleration mechanism for forward-directed ion acceleration at the rear surface is the Target Normal Sheath Acceleration (TNSA) mechanism[10]. Compared to subrelativistic intensity laser pulses, higher ion energies, up to ~5 MeV/nucleon, are observed with ultra-intense pulses.

In this article we report a characterisation of oxygen and palladium ion acceleration in the forward and backward directions, from heated Pd target foils, irradiated at ultra-high intensities. Ion energy and charge distributions are measured for a range of acceleration conditions, achieved by variation of laser pulse energy and duration.

Experimental

The petawatt beam line of the Vulcan laser[11] was used in this experiment. Pulse energies and durations in the range 40 to 375 J (on target) and 1.0 to 8.2 ps (FWHM), respectively, were used. The pulse duration was controlled by moving a grating in the pulse stretcher. An f/3 off-axis parabolic mirror was used to focus the *p*-polarised laser pulses onto palladium target foils at 45° angle of incidence. The peak laser pulse intensity was varied between 5×10^{19} and 5×10^{20} W/cm^2. The measured ratio of the level of the amplified spontaneous emission (ASE) relative to the peak intensity was 10^{-7} at a few nanoseconds and 10^{-6} at a few picoseconds prior to the peak of the pulse.

Under vacuum conditions typical of experiments of this type (~10^{-5} mbar), hydrocarbons and water vapour form thin contamination layers on the target surface. These provide a source of protons and carbon and oxygen ions. Having the largest charge-to-mass ratio (q/m), protons are accelerated more effectively than other, heavier, ions. The protons at the leading edge of the ion front screen the accelerating field acting on the heavier ions[4], and previous studies have shown that these ions are more efficiently accelerated when the source of the protons is removed[4,5,9]. Several methods are reported in the literature for reducing the hydrogenated contamination layers on the surfaces of the target, including laser ablation[12], ion sputtering[13] and target heating[4,5,7,9]. Target heating is reported to be the most effective[5] and we adopt this technique to ensure uniform cleaning of both target surfaces, to enable us to compare ion acceleration from both surfaces. Palladium target foils of 25 μm thickness were resistively heated to 1000°C for 10 minutes immediately prior to and during the

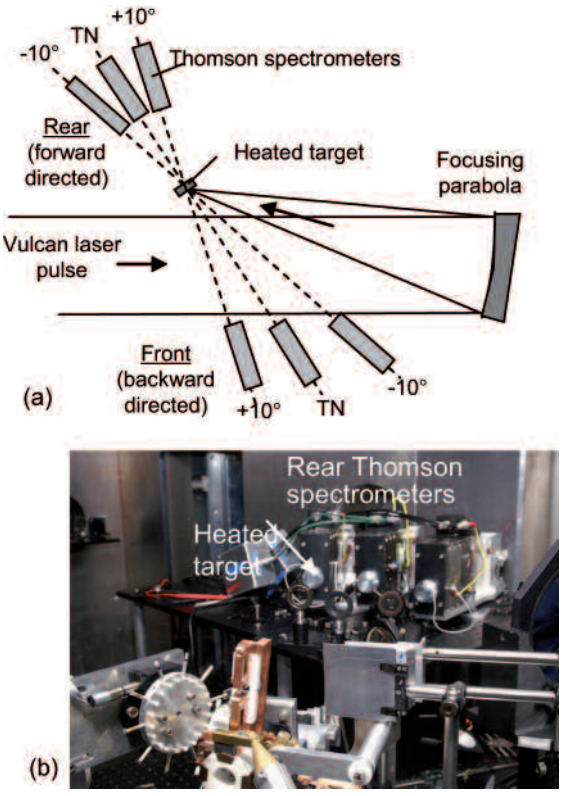

Figure 1. (a) Schematic diagram of the experiment. High power laser pulses are focused onto resistively heated Pd foil targets at an angle of 45°. The energy and charge-to-mass ratio of ions emitted along the target normal axis (TN) and at ±10°, at both the front and rear sides of the target, are characterised using Thomson spectrometers and CR-39 detector; (b) Photograph showing the heated target assembly and rear Thomson spectrometers.

laser shot. This effectively boils off most of the water and hydrocarbon molecules present on the surface, leaving only a thin oxide layer.

Six identical Thomson spectrometers were used as the primary diagnostic of ion acceleration. They were positioned on both sides of the target along the axis normal to the surface and at ±10° from the target normal, as shown in Figure 1. Thomson parabola spectrometers have parallel electric and magnetic fields to separate ions with different *q*/*m* into energy-dispersed tracks. The spectrometers employed in this study have been described previously[14]. The solid angles defined by the entrance apertures were in the range 5×10^{-9} to 2×10^{-8} Sr. CR-39 plastic track detector was positioned in the dispersion plane of the spectrometers to record the ion *q*/*m* and energy distributions. Each ion stopped in the CR-39 damages the plastic and after etching in NaOH solution a corresponding 'pit' (of typical diameter in the range 5 to 20 μm) is observed. An automated scanning microscope with pit recognition and analysis software[15] was used to digitise the spatial distribution of the pits. Ions of a given *q*/*m* produce a single signature parabolic track of pits in the CR-39. The measured tracks were identified by matching them to simulated ion trajectories, using the known electric and magnetic field distributions in the spectrometer[14]. The spatial distribution of the ions were mapped into energy versus *q*/*m* co-ordinates and the ion energy spectra extracted.

Results and Discussion

We measure the energy and charge distributions of ions detected in the spectrometers positioned at the front and rear sides of the target, for a range of laser pulse parameters, and find that the ion energy spectra measured on both sides of the target are broadly similar. In addition to the acceleration of palladium ions, we also detect oxygen ions, arising from the oxide layers on the target surfaces. We note that typically between 70% and 80% of the total ion energy is carried by palladium ions, with the remainder as ions from contaminants, principally oxygen. Example spectra for selected charge states of palladium are shown in figure 2. These spectra were measured along the target normal axis at the front of a heated Pd foil irradiated by a 122 J, 1 ps laser pulse. The spectra exhibit features similar to those previously reported[5,7,8], including an energy distribution which shifts to higher energies with increasing charge. The ions accelerated in both directions have similar maximum energies (multi-MeV/nucleon). Ions with charge states up to O^{6+} and Pd^{18+}, which correspond to closed shell electron configurations, are measured in the rear spectrometers at the highest laser intensity (5×10^{20} W/cm^2). Assuming field ionisation by barrier suppression is the dominant ionisation mechanism at the rear surface[4], a field strength of ~2×10^{12} V/m is needed to produce the observed ions[16]. Higher charge state ions are observed in the spectrometers positioned at the front side of the target, including fully stripped oxygen

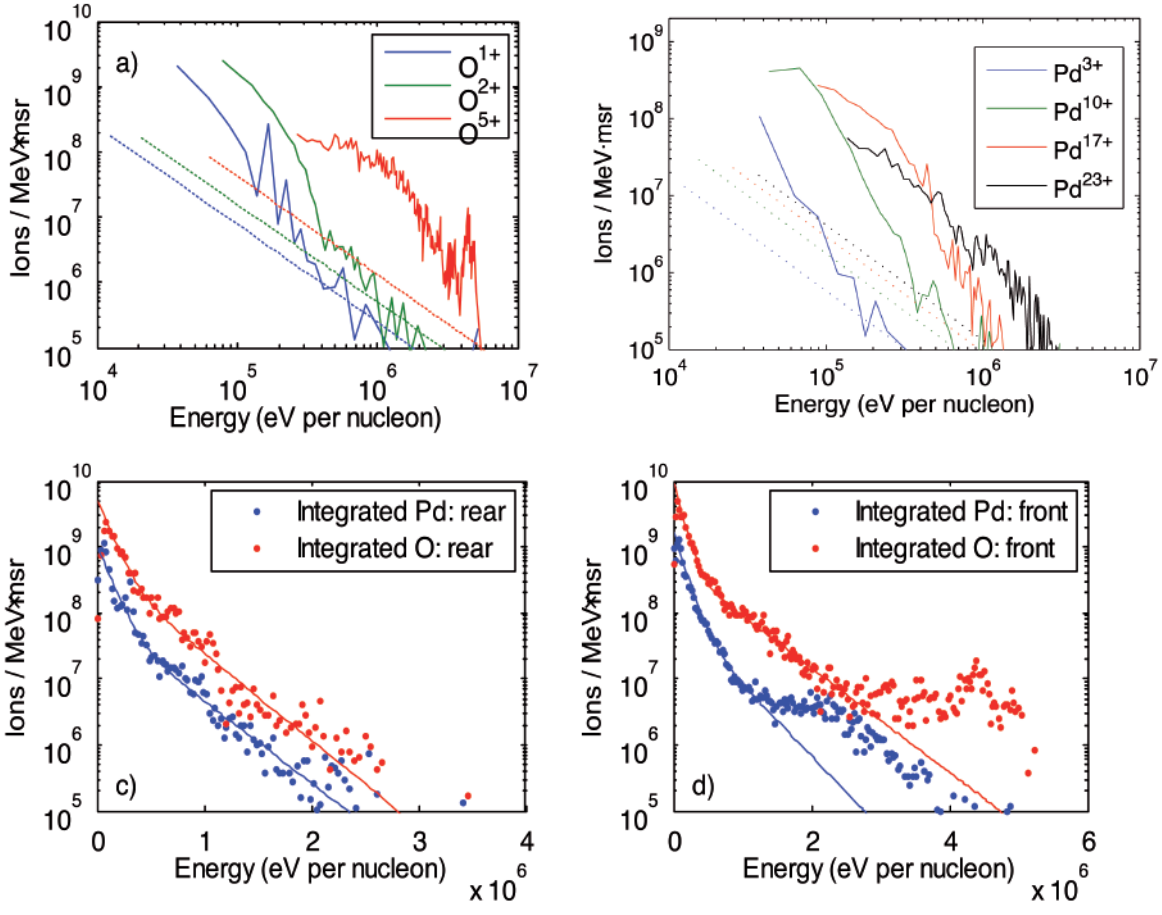

Figure 2. Example palladium ion energy spectra, measured along target normal at the front surface of a heated palladium target irradiated by a 122 J, 1 ps, 2×10^{20} W/cm^2 laser pulse. The solid lines are the measured spectra and the dashed lines correspond to the background level (lower detection threshold).

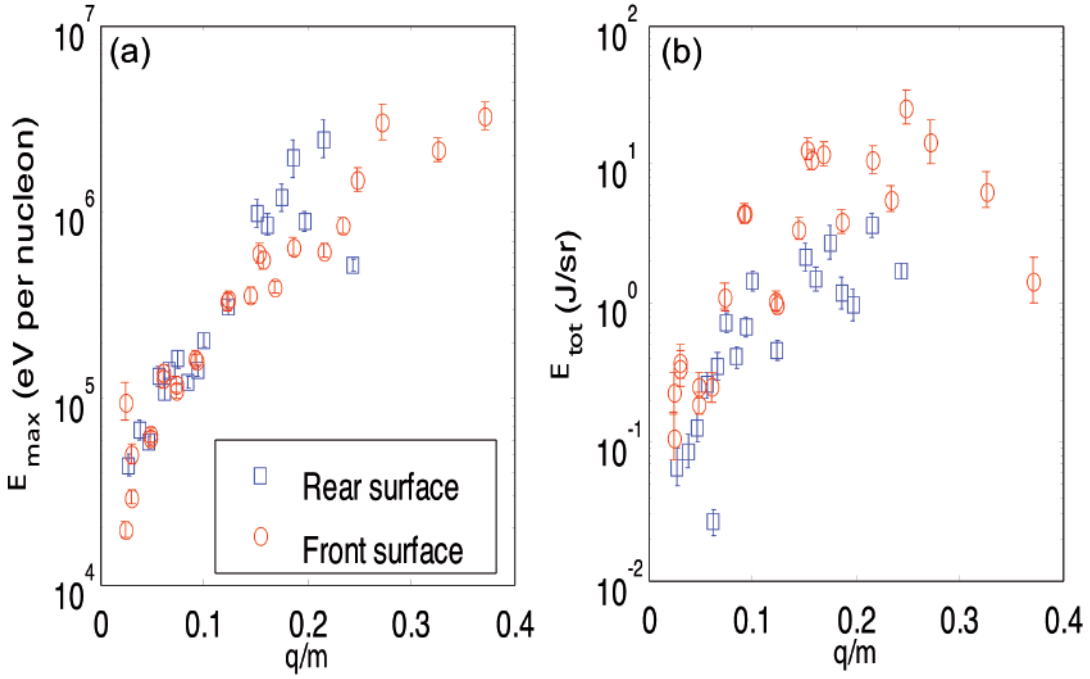

Figure 3. Maximum ion energy, E_{max}, (a) and total integrated ion energy, E_{tot}, (b) as a function of charge-to-mass (q/m) ratio, measured along the target normal axis at the front and rear sides of a heated palladium target irradiated by a 122 J, 1 ps, 2×10^{20} W/cm^2 laser pulse. The total energy in the ions emitted from the front surface is higher that the rear, and higher charge state ions are produced. Similar maximum ion energies are measured on both sides of the target.

and up to Pd^{30+}. The higher charge states are likely produced by the intense fields at the focus of the laser pulse itself or through collisional ionization in the hot plasma on the front surface of the target.

Figure 3 shows an example of the measured variation of the maximum detected ion energy, E_{max}, and the total energy of each ion species, E_{tot}, as a function of q/m. Similar scaling of both E_{max} and E_{tot} are observed on both sides of the target. We note that flux of ions measured at the target front surface is about a factor of five higher than measured at the rear.

A number of acceleration mechanisms may contribute to efficient backward-directed ion acceleration from the target front surface, including S-LPA [2,3,17]. A mechanism similar to TNSA arising from the Debye sheath formed at the front surface of the target (in addition to the rear) may also contribute. Electron refluxing within the target foil [18] is expected as the distance travelled by relativistic electrons during the laser pulse duration, ~300 μm, is much larger than twice the target thickness, and hence the quasistatic electric fields formed on both surfaces will be enhanced. A steepening of the density gradient at the focus of the ultraintense laser pulse may further aid front surface acceleration.

In order to determine to what extent the measured scaling of ion energy with charge (figure 3(a)) depends on the initial charge state distribution, we model the ion expansion from the target rear surface using the one dimensional explicit particle-in-cell (PIC) code, described in reference [19]. The simulation space involves a grid of 20000 spatial points with a cell size of 2 nm, and a linear interpolation is used for particle and grid weighting. The target has a top-hat density profile, with an ion density of 2×10^{28} m^{-3} (i.e. ~0.3 times the density of Pd) and a thickness of 4 μm. The electron density is set to give overall charge neutrality. The ion and electron densities are kept sufficiently low so that the simulation run-time is feasible. The 'laser' pulse duration is 200 fs (FWHM) with a sin^2 envelope function, wavelength 1 μm and intensity 2×10^{20} W/cm^2. The pulse duration and target thickness are scaled by a similar order. The dynamics of six Pd ion species (mass equal to 1.78×10^{-25} kg) with charges 3, 5, 8, 11, 19, and 23 are modelled in each simulation.

Results from four of the simulations are shown in figure 4(a) (coloured lines with symbols), together with the experimental measurement along target normal at the target rear. The blue line corresponds to the results when the initial charge population distribution is close to the experimentally measured distribution. The green line results

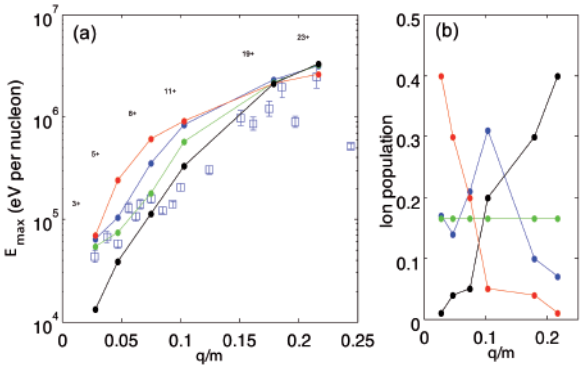

Figure 4. (a) Maximum ion energy as a function of ion charge-to-mass ratio from numerical PIC simulations using the model described in the main text. The various colours correspond to the ion charge state populations shown in (b). The blue squares in (a) are the experimental results from figure 3(a), reproduced for comparison.

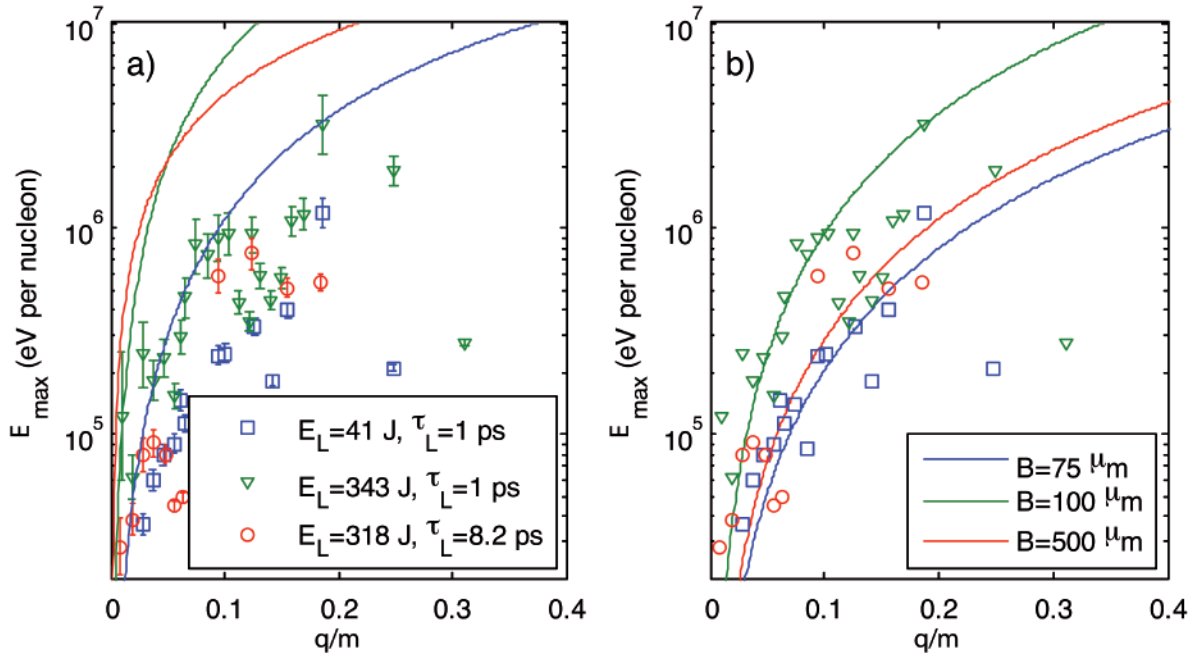

Figure 5. Maximum ion energy, E_{max}, as a function of ion charge-to-mass ratio, for three experimental conditions: blue, 41 J, 1 ps (6×10^{19} W/cm^2); green, 343 J, 1 ps (5×10^{20} W/cm^2); red, 318 J, 8.2 ps (5×10^{19} W/cm^2). The solid curves are the predictions of the Schreiber model for the three sets of laser parameters (a) for fixed sheath radius B=30 μm and (b) with B as a fitting parameter.

when the ion population is equally distributed across the six charges sampled. The red and the black lines correspond to the extreme cases in which the population distribution is weighted towards the low and high charge states, respectively. The ion population distribution functions for all four simulation runs are shown in figure 4(b). We note that all four simulations results converge for the highest charge ions and that when the population is more heavily weighted towards higher q/m ions, the maximum energy of the lowest q/m ions decreases significantly. Since the field decays as $1/\omega_{pi}t$, where ω_{pi} (the ion plasma frequency) $\propto\sqrt{q}$ [20], with increasing q the electric field decays more rapidly and the lower q/m species (Pd^{5+}) is accelerated to successively lower energy. In this way the ion energy scaling with q/m is likely to be a complicated function of the ionisation dynamics and the ionisation charge distribution.

A number of analytical models exist for ion acceleration driven by high power lasers. Schreiber *et al.* [21] describes an analytical model which gives good agreement with experimental measurements of ion acceleration as a function of charge, in the intensity range up to 6×10^{19} W/cm^2. We apply this model to determine the predicted scaling of the maximum ion energies as a function of q/m at the higher laser intensities explored experimentally in the present study, as shown in figure 5. Specifically, we calculate the maximum ion energy as a function of q/m for the three sets of laser parameters at the extremes of our experimental parameter range and find that the predicted energies are higher than experimentally observed, as shown in figure 5(a). We note however that a sheath radius B=30 μm radius is used in the model (calculated based on the laser focal spot size and the estimated cone angle of electron transport within the target). The actual sheath size for the interaction of picosecond duration pulses with a thin foil can be much larger due to refluxing [18] of hot electrons, with a transverse velocity component, within the foil. Ion sources sizes of the order of 100 to 200 μm have been measured using proton probing of picosecond pulse interactions with foil targets [22]. Next we use the electron sheath size as a fitting parameter and find reasonable agreement between the model and experiment when large sheath sizes are inferred, as shown in figure 5(b). The two sets of experimental data at 1 ps pulse duration are reproduced quite well by the model when B is of the order of 75 to 100 μm. The longer pulse duration measurements require a much larger sheath, with radius of the order of 500 μm, for the Schreiber model to provide a good fit. This is consistent with the idea of increased lateral spreading of the electron sheath due to the increased number of cycles of refluxing electrons for the longer pulse duration.

Summary

We have experimentally investigated ion acceleration driven by petawatt-class laser pulse interactions with resistively heated target foils. We find that ions are accelerated to multi-MeV/nucleon energies in both directions, and that larger numbers and higher charges of ions are accelerated from the target front surface.

We have applied a numerical PIC model [19] and an analytical model [21] to our measurement of the scaling of the maximum energy of ions accelerated at the target rear surface as a function of ion charge-to-mass ratio. Using the PIC model we have investigated the sensitivity of the ion energy on the charge population distribution. Application of the analytical model to the measured ion energy as a function of q/m infers a large ion source size on the target rear surface, which increases with laser pulse duration. This is consistent with increased lateral spreading of the hot electron population due to increased recirculation within the foil, for the longer laser pulse duration.

Acknowledgements

The authors would like to acknowledge the Vulcan laser group. The authors are also grateful for the use of computing resources provided by STFC's e-Science facility. FL and OL acknowledge support from the COST P-14 Action.

References

1. M. Borghesi *et al*., *Fusion Science and Technology* **49**, 412 (2006).
2. J. Badziak, *Opto-electronics Review* **15**, 1 (2007).
3. J. Badziak *et al*., *Applied Physics Letters* **79**, 21 (2001).
4. M. Hegelich *et al*., *Physical Review Letters* **89**, 085002 (2002).
5. B. M. Hegelich *et al*., *Physics of Plasmas* **12**, 056314 (2005).
6. E. Brambrink *et al*., *Physical Review Letters* **96**, 154801 (2006).
7. J. Schreiber *et al*., *Applied Physics B: Lasers and Optics* **79**, 1041 (2004).
8. E. L. Clark *et al*., *Physical Review Letters* **85**, 1654 (2000).
9. P. McKenna *et al*., *Physical Review E* **70**, 036405 (2004).
10. S. C. Wilks *et al*., *Physics of Plasmas* **8**, 542 (2001).
11. C. Hernandez-Gomez *et al*., *Journal de Physique IV* **133**, 555 (2006).
12. H. Schwoerer *et al*., *Nature* **439**, 445 (2006).
13. M. Allen *et al*., *Physics of Plasmas* **10**, 3283 (2003).
14. D. Carroll *et al*., Central Laser Facility, Rutherford Appleton Laboratory Annual Report 2005-06 **26**.
15. TASL-IMAGE, Track Analysis Systems Limited; Details online at www.tasl.co.uk
16. T. A. Carlson *et al*., *Atomic Data* **2**, 63 (1970).
17. J. Badziak *et al*., *Laser and Particle Beams* **17**, 323 (1999).
18. Y. Sentoku *et al*., *Physics of Plasmas* **10**, 2009 (2003).
19. A. P. L. Robinson *et al*., *Plasma Physics and Controlled Fusion* **49**, 373 (2007).
20. P. Mora, *Physical Review Letters* **90**, 185002 (2003).
21. J. Schreiber *et al*., *Physical Review Letters* **97**, 045005 (2006).
22. M. Borghesi *et al*., *Physical Review Letters* **92**, 055003 (2004).